

Multichannel adaptive deconvolution based on streaming prediction-error filter^a

^aPublished in Journal of Geophysics and Engineering, 18, 825-833, (2021)

Qinghan Wang, Yang Liu, Cai Liu, and Zhisheng Zheng

ABSTRACT

Deconvolution mainly improves the resolution of seismic data by compressing seismic wavelets, which is of great significance in high-resolution processing of seismic data. Prediction-error filtering/least-square inverse filtering is widely used in seismic deconvolution and usually assumes that seismic data is stationary. Affected by factors such as earth filtering, actual seismic wavelets are time- and space-varying. Adaptive prediction-error filters are designed to effectively characterize the nonstationarity of seismic data by using iterative methods, however, it leads to problems such as slow calculation speed and high memory cost when dealing with large-scale data. We have proposed an adaptive deconvolution method based on a streaming prediction-error filter. Instead of using slow iterations, mathematical underdetermined problems with the new local smoothness constraints are analytically solved to predict time-varying seismic wavelets. To avoid the discontinuity of deconvolution results along the space axis, both time and space constraints are used to implement multichannel adaptive deconvolution. Meanwhile, we define the parameter of the time-varying prediction step that keeps the relative amplitude relationship among different reflections. The new deconvolution improves the resolution along the time direction while reducing the computational costs by a streaming computation, which is suitable for handling nonstationary large-scale data. Synthetic model and filed data tests show that the proposed method can effectively improve the resolution of nonstationary seismic data, while maintaining the lateral continuity of seismic events. Furthermore, the relative amplitude relationship of different reflections is reasonably preserved.

INTRODUCTION

Thin interbedded reservoirs and subtle reservoirs with complex lithology are becoming key areas of seismic exploration and development. Conventional seismic data is difficult to accurately characterize the thin reservoir, therefore, improvement of seismic resolution is a persistent problem in seismic exploration. Two major categories improving the vertical resolution of seismic data include deconvolution (ver der Baan, 2008, 2012; Margrave et al., 2011; Li et al., 2013) and inverse Q filtering (Wang, 2002,

2006), and those techniques can effectively broaden the frequency bandwidth and improve the accuracy of seismic data interpretation, especially in the identification of thin reservoir. The inverse Q filtering method compensates the attenuation of wave amplitude and fixes the phase distortion caused by the absorption of subsurface media; however, the correction depends on the accuracy of the quality factor Q. Predictive deconvolution method improves the resolution of seismic data by compressing seismic wavelet, which depends on the assumptions of minimal phase wavelet and whitening reflection coefficients. Thus, predictive deconvolution is suitable for vibroseis seismic data (Ristow and Jurczyk, 1975).

Prediction-error filtering (PEF) or least-square inverse filtering has been applied in seismic deconvolution for decades, and it has proved its effectiveness for resolution improvement and multiple elimination. The theory of predictive deconvolution was introduced by Robinson (1957, 1967). Peacock and Treitel (1969) proved the effectiveness of predictive deconvolution for enhancing resolution and suppressing periodic multiples. To take full advantage of the spatial characteristics of seismic data and suppress noise, several authors developed multichannel predictive deconvolution (Claerbout, 1992; Porsani and Ursin, 2007; Li et al., 2016). The traditional deconvolution method is designed under the assumption of stationary data and becomes less effective because seismic data are nonstationary in nature. Clark (1968) proposed a nonstationary deconvolution in time domain based on optimal Wiener filtering. Wang (1969) gave the criteria for determining the optimal length of the filtering window on the assumption of a piecewise stationary. Griffiths et al. (1977) proposed an adaptive predictive deconvolution method that adaptively updates the filter coefficients for each data point. Koehler and Taner (1985) proposed a generalized mathematical theory of time-varying deconvolution and used the conjugate gradient algorithm to calculate the filter coefficients. Prasad and Mahalanabis (1980) compared three adaptive deconvolution methods and demonstrated that all three methods perform better than traditional predictive deconvolution when dealing with nonstationary data. Liu and Fomel (2011) obtained smoothly nonstationary PEF coefficients by solving a global regularized least-squared problem, however, iterative approach leads to slow computation speed and high memory cost. Fomel and Claerbout (2016) proposed the concept of streaming computation, which can adaptively update the filter coefficients without iteration, and the properties of nonstationary representation and low computational cost are useful for the single-channel deconvolution model and random noise attenuation of seismic data (Liu and Li, 2018). To improve the resolution effectively for nonstationary seismic data, in this paper, we design a multichannel adaptive deconvolution method based on the streaming prediction error filter in time-space domain. The time and space constraints added to the objective function can guarantee the continuity of deconvolution results in space direction, and the relationship between the prediction step and wavelet frequency reasonably improve the fidelity of the reflection coefficients in the deconvolution result.

This paper is organized as follows. First, we introduce the streaming computation for adaptive PEF. Then, we propose the improved streaming PEF method that involves spatial constraints and time-varying prediction step. Finally, the synthetic

data and real data are used to demonstrate that the proposed method can be effective and efficient in vertical resolution improvement of nonstationary seismic data.

THEORY

According to the theory of predictive deconvolution, time-varying filter coefficients are designed to predict nonstationary seismic data, which can be expressed as a nonstationary autoregressive equation,

$$r(t) = s(t) - \sum_{n=1}^N c_n(t)s(t-n+1-\alpha) = s(t) - \mathbf{S}^T \mathbf{C}, \quad (1)$$

where α is the prediction step, $s(t)$ and $r(t)$ are the original seismic data and prediction error, respectively, $\mathbf{S}^T = [s(t-\alpha), s(t-1-\alpha), \dots, s(t-N+1-\alpha)]$, which represents the causal translation of $s(t)$, all prediction coefficients $\mathbf{C} = [c_1(t), c_2(t), \dots, c_N(t)]$ are estimated in a time variant manner, and N denotes the length of the predictive filter. The filter coefficients are obtained by solving the least-squares problem:

$$\min_{\mathbf{C}} \| s(t) - \mathbf{S}^T \mathbf{C} \|_2^2, \quad (2)$$

which is a classical underdetermined problem. The local smoothness constraints with streaming computation (Fomel and Claerbout, 2016) avoids the problem of high computational costs associated with iterative approaches. One can assume that the filter coefficients corresponding to two adjacent data stay close, and the autoregressive equation can be expressed by an overdetermined equation as

$$\begin{bmatrix} s(t-\alpha) & s(t-1-\alpha) & \cdots & s(t-N+1-\alpha) \\ \epsilon_t & 0 & \cdots & 0 \\ 0 & \epsilon_t & \cdots & 0 \\ \vdots & \vdots & \ddots & \vdots \\ 0 & 0 & \cdots & \epsilon_t \end{bmatrix} \times \begin{bmatrix} c_1(t) \\ c_2(t) \\ \vdots \\ c_N(t) \end{bmatrix} = \begin{bmatrix} s(t) \\ \epsilon_t c_1(t-1) \\ \epsilon_t c_2(t-1) \\ \vdots \\ \epsilon_t c_N(t-1) \end{bmatrix}. \quad (3)$$

Equation 3 can be written in terms of a shortened block-matrix notation

$$\begin{bmatrix} \mathbf{S}^T \\ \epsilon_t \mathbf{I} \end{bmatrix} \mathbf{C} = \begin{bmatrix} s(t) \\ \epsilon_t \overline{\mathbf{C}}_t \end{bmatrix}, \quad (4)$$

where $\overline{\mathbf{C}}_t = [c_1(t-1), c_2(t-1), \dots, c_N(t-1)]$, which represents the previous filter coefficient on time axis, ϵ_t is the constant scale parameter controlling the variability of two adjacent filter coefficients in the time axis, and \mathbf{I} is the identity matrix. Consider a multichannel seismic data, an extra spatial constraint can introduce to the smoothness of the time-varying filter coefficients along the space axis. The new prediction filter can be expressed in the form of a block matrix as

$$\begin{bmatrix} \mathbf{S}_m^T \\ \epsilon_t \mathbf{I} \\ \epsilon_x \mathbf{I} \end{bmatrix} \mathbf{C} = \begin{bmatrix} s_m(t) \\ \epsilon_t \bar{\mathbf{C}}_t \\ \epsilon_x \bar{\mathbf{C}}_x \end{bmatrix}, \quad (5)$$

where $s_m(t)$ and $\mathbf{S}_m^T = [s_m(t - \alpha), s_m(t - 1 - \alpha), \dots, s_m(t - N + 1 - \alpha)]$ represent the multichannel data with space index m and the causal translation of the m th seismic trace, ϵ_x is the scalar regularization parameter in the space axis, and $\mathbf{C} = [c_1^m(t), c_2^m(t), \dots, c_N^m(t)]$ is the time-varying filter coefficient with space-varying index m . The previous filter $\bar{\mathbf{C}}_t = [c_1^m(t - 1), c_2^m(t - 1), \dots, c_N^m(t - 1)]$ on the time axis and the previous filter on space axis $\bar{\mathbf{C}}_x = [c_1^{m-1}(t), c_2^{m-1}(t), \dots, c_N^{m-1}(t)]$ are similar to the current filter $\mathbf{C} = [c_1^m(t), c_2^m(t), \dots, c_N^m(t)]$.

Assuming that adjacent filter coefficients are similar, the current filter coefficients at a certain point can be constrained by the adjacent filter coefficients in both time and space directions, and the regularization constraint terms are $\epsilon_t^2 \|\mathbf{C} - \bar{\mathbf{C}}_t\|_2^2$ and $\epsilon_x^2 \|\mathbf{C} - \bar{\mathbf{C}}_x\|_2^2$. ϵ_t and ϵ_x are weights for regularization constraint terms along time and space directions, respectively, which control the similarity of the adjacent filter coefficients. In this case, the underdetermined problem is transformed into an overdetermined problem. The filter coefficients are calculated by solving the regularized autoregression problem

$$\min_{\mathbf{C}} \|\mathbf{C} - \mathbf{S}_m^T \mathbf{C}\|_2^2 + \epsilon_t^2 \|\mathbf{C} - \bar{\mathbf{C}}_t\|_2^2 + \epsilon_x^2 \|\mathbf{C} - \bar{\mathbf{C}}_x\|_2^2, \quad (6)$$

the least-squares solution of equation 6 is

$$\mathbf{C} = (\mathbf{S}_m \mathbf{S}_m^T + \epsilon_t^2 \mathbf{I} + \epsilon_x^2 \mathbf{I})^{-1} (s_m(t) \mathbf{S}_m + \epsilon_t^2 \bar{\mathbf{C}}_t + \epsilon_x^2 \bar{\mathbf{C}}_x). \quad (7)$$

The Sherman-Morrison formula in linear algebra (Hager, 1989) is able to directly transform the inverse matrix in equation 7 without iterations:

$$(\mathbf{S}_m \mathbf{S}_m^T + \epsilon_t^2 \mathbf{I} + \epsilon_x^2 \mathbf{I})^{-1} = \frac{1}{\epsilon_t^2 + \epsilon_x^2} \left(\mathbf{I} - \frac{\mathbf{S}_m \mathbf{S}_m^T}{\epsilon_t^2 + \epsilon_x^2 + \mathbf{S}_m^T \mathbf{S}_m} \right), \quad (8)$$

where \mathbf{S}_m is a column vector and \mathbf{S}_m^T is the transpose of \mathbf{S}_m . Substituting equation 8 into 7, the streaming PEF coefficients can be calculated as

$$\mathbf{C} = \bar{\mathbf{C}} + \left(\frac{s_m(t) - \mathbf{S}_m^T \bar{\mathbf{C}}}{\epsilon^2 + \mathbf{S}_m^T \mathbf{S}_m} \right) \mathbf{S}_m, \quad (9)$$

where

$$\begin{cases} \epsilon^2 = \epsilon_t^2 + \epsilon_x^2 \\ \bar{\mathbf{C}} = \frac{\epsilon_t^2 \bar{\mathbf{C}}_t + \epsilon_x^2 \bar{\mathbf{C}}_x}{\epsilon^2} \end{cases}. \quad (10)$$

Equation 9 shows that the adaptive coefficients get updated by adding a scaled version of the data, and the scale is proportional to the streaming prediction error.

Updating the filter coefficients requires only elementary algebraic operation without iteration.

According to the definition of prediction error (equation 1) and prediction coefficients (equation 9), the deconvolution result of streaming PEF can be expressed as

$$r_m(t) = s_m(t) - \mathbf{S}_m^T \mathbf{C} = \frac{\epsilon^2 (s_m(t) - \mathbf{S}_m^T \bar{\mathbf{C}})}{\epsilon^2 + \mathbf{S}_m^T \mathbf{S}_m}. \quad (11)$$

In this paper, we select the minimum-phase wavelet as the source wavelet to verify the effectiveness of the proposed deconvolution method. The minimum-phase wavelet can be expressed as

$$w(t) = e^{-(2\pi f_m t/25)^2} \sin(2\pi f_m t), \quad (12)$$

where f_m is the dominant frequency of the wavelet.

The minimum-phase wavelet (figure 1a) and the sequence of reflection coefficients (figure 1b) generate a simple 1D convolution model (figure 1c), where the wavelet frequencies corresponding to every two reflection coefficients with opposite amplitude are selected to be 45 Hz, 35 Hz, 25 Hz, and 20 Hz, respectively. Figure 1d is the result by using the streaming PEF deconvolution ($N = 10$, $\epsilon_t = 0.2$, and $\alpha = 1$). The streaming PEF deconvolution method effectively improve the time resolution, however, the relative amplitude relationship among different reflections has been changed, which occur more in predictive deconvolution methods. Notice that the amplitude distortion is related to the dominant frequency of the wavelet: the lower dominant frequency is, the worse amplitude fidelity is shown because the peak amplitude of minimum-phase wavelets is hard to happen in the first sample point.

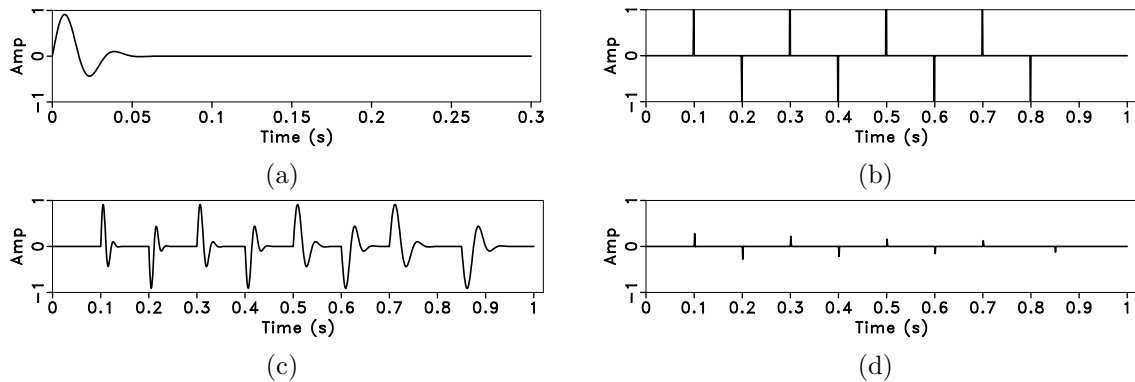


Figure 1: Analysis of amplitude distortion for streaming PEFs. Minimum-phase wavelet (a), the reflectivity (b), the nonstationary synthetic seismic trace (c), and the deconvolution result by using streaming PEF with constant prediction step (d).

The red line in figure 2 represents the theoretical curve of sample number between the start point and peak-amplitude point of minimum-phase wavelets, which is the function of the dominant frequency. We select an empirical equation to fit the curve

as follows:

$$gap = Round\left(\frac{b}{f \times \Delta t}\right), \quad (13)$$

where $Round$ represents a rounding function, gap is the sample number between the start point and the peak-amplitude point, Δt is the time interval, and b is a constant. One can determine parameter b from any point in the curve, e.g., b is selected to be 0.232 in figure 2, where the dominant frequency is 1 Hz, the sample interval is 1 ms, and the gap is 232. The blue dotted line calculated by equation 12 reasonably fits the red theoretical curve. Therefore, we further design the streaming PEF deconvolution method with the time-varying prediction step to preserve the relative amplitude relationship of different reflection coefficients. The adaptive prediction step is selected to be the parameter gap , which makes the prediction error after deconvolution close to the maximum amplitude value of the original wavelet. The new streaming deconvolution residual is rewritten as follow:

$$r(t) = s(t) - \sum_{n=1}^N c_n(t)s(t - n + 1 - \alpha(t)), \quad (14)$$

where $\alpha(t)$ is the time-varying prediction step, which is determined by a time-varying gap value

$$\alpha(t) = gap(t) = Round\left(\frac{b}{f(t) \times \Delta t}\right), \quad (15)$$

where $f(t)$ is the time-varying local frequency obtained by the shaping regularization (Fomel, 2007a). The instantaneous frequency calculated instantaneously at each signal point sometimes appears noisy and contains physically unreasonable negative frequency, so Fomel (2007a) defined the local frequency by using the shaping regularization (Fomel, 2007b) to constrain the linear inversion problem. When calculating the local frequency, the continuity and smoothness of the local frequency can be controlled only by adjusting a smooth radius parameter, and the local frequency shows better physical meaning than the instantaneous frequency.

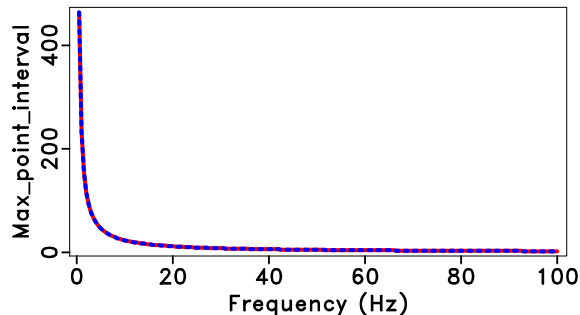


Figure 2: Parameter gap curve of minimum phase wavelet with different frequencies.

Figure 3a shows the local frequency calculated from the synthetic trace (figure 1c), and the time-varying prediction steps (figure 3b) are obtained according to equation 14, where the parameter b is 0.232 and the time interval is 1 ms. Figure 3c shows

the result processed by the streaming PEF deconvolution with the time-varying prediction step. Compared with original data (dotted line in figure 3c), the proposed method keeps the relative amplitude relationship in the deconvolution result (solid line in figure 3c) at the cost of a lower resolution improvement.

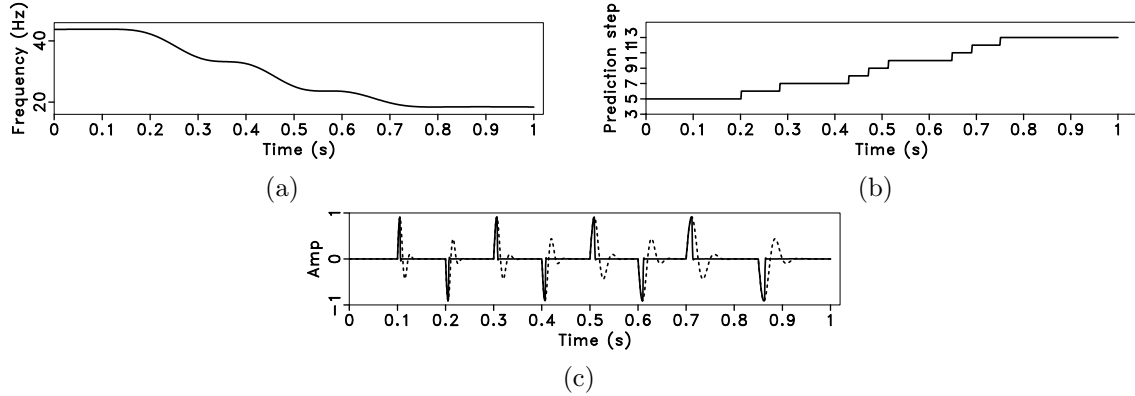


Figure 3: The deconvolution result by using the streaming PEF with time-varying prediction steps. The local frequency (a), time-varying prediction step (b), the deconvolution result with the proposed method (solid line), which is compared with the original trace (dotted line) (c).

The proposed method mainly includes four parameters: the filter length (N), time constraint factor (ϵ_t), spatial constraint factor (ϵ_x) and constant b . According to the experiment, a reasonable deconvolution results can be obtained when $N \leq 10$. The constraint factors ϵ_t and ϵ_x are the key parameters for the proposed method. The denominator in equation 9 suggests that ϵ_t^2 and ϵ_x^2 should have the same order of the magnitude as $\mathbf{S}_m^T \mathbf{S}_m$. Too small a constraint factor would make the deconvolution results unstable, and too large a constraint factor would lead to the filter coefficients not being updated effectively. When the filter coefficients are constrained only in the time direction, it is only necessary to set the spatial constraint factor to zero ($\epsilon_x = 0$). In theory, the b value is the ratio of the peak-amplitude time to the period of the wavelet. For minimum-phase wavelets, b is typically less than 0.25.

Like the traditional predictive deconvolution, the relative amplitude relationship of the results that are generated by streaming PEF deconvolution with constant prediction step is not consistent with the original data, so we introduce the time-varying prediction step and derive its empirical formula. After adding the time-varying prediction step, the amplitude of the deconvolution result of the synthetic model (figure 3) tends to be consistent with the true amplitude of the original data. However, the actual seismic data is complex due to the earth absorption attenuation and other factors, so the amplitude of deconvolution results is not true amplitude, but its relative amplitude relationship is closer to the original data.

Since the proposed method can adaptively update the filter coefficients without iteration and characterize the nonstationary properties of the data, both the storage and computational cost of the filters are less than those of the adaptive predictive

filtering methods based on the iterative algorithms. Table 1 compares the storage and computational cost of the different methods.

The proposed filter is constrained in both the time and space directions while the filter is still one-dimensional, that is, the multichannel adaptive deconvolution technology is based on the streaming PEF with one-dimensional structure and two-dimensional constraints. To ensure the stability of the calculation, the first boundary trace only uses the time constraint condition to compute the streaming PEF coefficients, and the constraints in both space and time directions are added to the other trace. An extension of the proposed method to 3D is straightforward and provides a fast adaptive multichannel deconvolution implementation for high-dimensional seismic data.

Method	Storage	Cost
Stationary PEF	$O(N_a)$	$O(N_a^2 N_t)$
1D nonstationary PEF with iterative algorithm	$O(N_a N_t)$	$O(N_a N_t N_{iter})$
1D streaming PEF	$O(N_a)$	$O(N_a N_t)$
2D streaming PEF	$O(N_a N_t)$	$O(N_a N_t N_x)$

Table 1: Rough cost comparison among the different PEF estimation methods. N_a is the the filter size, N_t is the data length in the time direction, N_x is the data length in the space direction, N_{iter} is the number of iterations.

NUMERICAL EXAMPLES

1D attenuation model

We start with a 1D synthetic example with the quality factor Q attenuation according to the modified Kolsky model (Wang and Guo, 2004; Wang, 2008). In this model, the phase velocity is defined as

$$\frac{1}{v(\omega)} = \frac{1}{v_r} \left(1 - \frac{1}{\pi Q_r} \ln \left| \frac{\omega}{\omega_h} \right| \right) \approx \frac{1}{v_r} \left| \frac{\omega}{\omega_h} \right|^{-\gamma}, \quad (16)$$

where $\gamma = \frac{1}{\pi Q_r}$, Q_r and v_r are the quality factor and phase velocity at a reference frequency ω_r (the dominant frequency in general), ω_h is the tuning frequency. We generate a time-varying trace (figure 4b), where the dominant frequency of the unattenuated minimum-phase wavelet is 40 Hz, the time interval is 1 ms, and the Q value is 30. Figure 4a shows the actual reflectivity. For comparison, we use the traditional predictive deconvolution to squeeze all wavelets (figure 5a), the filter length N is ten and the prewhitening factor is 0.0001. The traditional method produces a reasonable result at the high-frequency locations; however, the predictive deconvolution still loses part of the original amplitudes. We design the streaming PEF deconvolution

with a constant prediction step ($N = 3$, $\epsilon_t = 1.5$, and $\alpha = 1$) to further handle the variability of wavelet (figure 5c). The streaming PEF residual visually shows a result similar to the traditional method, however, a close-up comparison between the traditional deconvolution (figure 5b) and the proposed deconvolution (figure 5d) shows an obvious resolution difference, which proves better nonstationary characteristics of the streaming PEF.

Next, we improve the adaptive deconvolution result by involving the time-varying prediction step, and the result is shown in figure 6. Figures 6a and 6b show the decay of local frequency and the time-varying prediction step by using equation 14 where $b = 0.06$, respectively. Figure 6c shows that the proposed method keeps the relative amplitude relationship without auto gain correction (AGC) and the time resolution is reasonably enhanced. Figure 6d shows amplitude spectrum of the synthetic data before and after deconvolution, where the grey line is the original synthetic data and the black line is the deconvolution result. It can be seen from figure 6d that the amplitude spectrum broadens after the deconvolution.

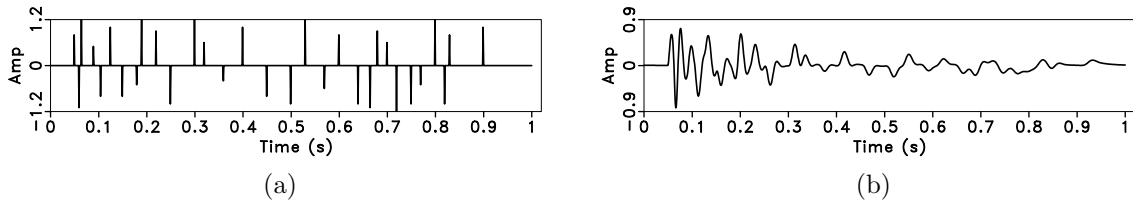


Figure 4: A synthetic seismic trace example. The reflectivity (a), synthetic trace with Q attenuation (b).

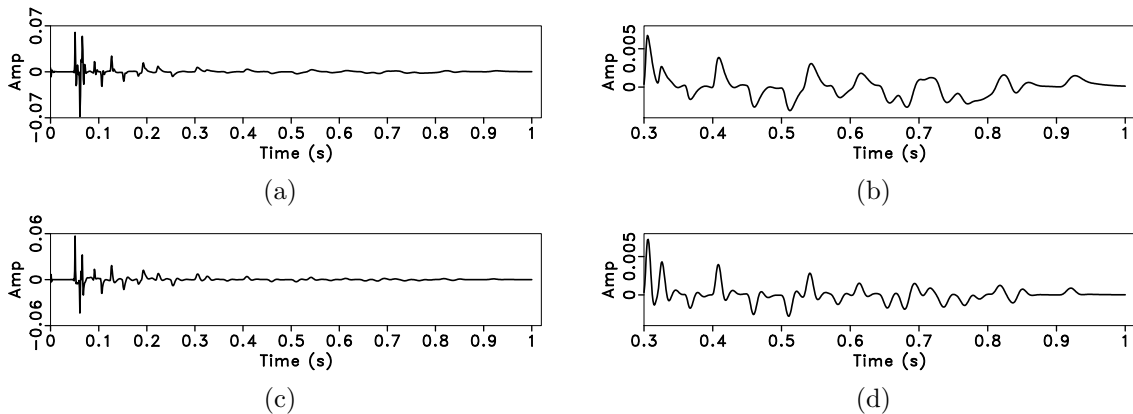


Figure 5: Deconvolution results by using different methods. Traditional predictive deconvolution (a), local display of (a) (b), streaming PEF deconvolution (c), local display of figure (c) (d).

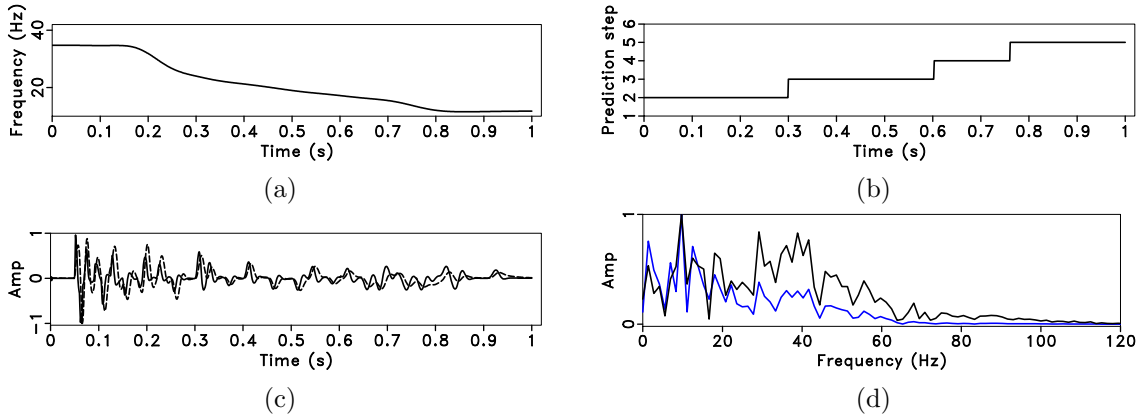


Figure 6: Deconvolution by using streaming PEF with time-varying prediction steps. Local frequency (a), time-varying prediction step (b), the deconvolution result with the proposed method (solid line), which is compared with the original trace (dotted line) (c), amplitude spectrum (The grey line is the original data, and the black line is the deconvolution result) (d).

2D wedge model

The second example is shown in figure 7a. We use a 2D benchmark wedge model to prove the necessity of the spatial constraint for the streaming PEF deconvolution. The velocity of the wedge in the model is 10 kft/s, and the velocity of the upper and lower media is 20 kft/s, therefore, the wave impedance corresponding to the top and bottom interfaces of the wedge are reversed. The minimum-phase wavelet with the dominant frequency of 30 Hz is selected to create the synthetic data (figure 7b), where the wavelet of the top and bottom interfaces appears interference started from the 45th trace. The synthetic data are firstly processed using the traditional predictive deconvolution method (the filter length is 3) and the regularized non-stationary autoregressive (RNA) method (the filter length is 3) based on the iterative algorithm (Liu and Fomel, 2011), and the deconvolution results are shown in figures 7c and 7d, respectively. Due to the model is stationary data, both methods can effectively improve the resolution and distinguish the top and bottom interfaces of the wedge model, but the traditional predictive deconvolution method is not suitable for processing nonstationary data (see figure 5) and iterative RNA deconvolution produces high computational cost. Then we design a streaming PEF with 3 (time) coefficients, the prediction step $\alpha = 1$, and the time constraint factor $\epsilon_t = 0.2$ for each sample to further verify the effectiveness of the spatial constraint. Figures 7e and 7f show the streaming PEF deconvolution results without spatial constraint ($\epsilon_x = 0$) and with spatial constraint ($\epsilon_x = 0.5$), respectively. Both single-channel and multichannel deconvolution improve the vertical resolution, however, the result without spatial constraint appears with unstable fluctuation and spatial discontinuity, especially at rectangle location in figure 7e. The spatial constraint can effectively reduce the fluctuation and enhance the structural continuity of deconvolution result. Meanwhile,

the computation time of the traditional method, iterative method, single-channel, and multichannel streaming PEF deconvolution method is 0.011 s, 0.220 s, 0.011 s, and 0.012 s, respectively.

Field example

For the field data test, we use a 2D poststack section with time interval of 2 ms. The input is shown in figure 8a. For comparison, we apply the traditional predictive deconvolution (the filter length is 6) and the iterative method (the filter length is 6) to enhance the time resolution, as shown in figures 8b and 8c. Figure 8d shows a processing result using the proposed streaming PEF deconvolution method. The streaming PEF parameters are 6 (N), 0.032 (b), 25000 (ϵ_t), and 10000 (ϵ_x). The computation time of traditional, iterative method, and streaming PEF deconvolution methods are 0.024 s, 18.767 s, and 1.018 s, respectively, however, the traditional deconvolution method cannot enhance the time resolution at all time because of non-stationary of the field data. The proposed deconvolution and iterative methods can improve the vertical resolution at different times, so both methods are more suitable for processing nonstationary data. Moreover, compared with the traditional and iterative methods, the proposed method can better keep the continuity of events. Furthermore, we select a part of the data near to the reservoir layer from 3-3.5 s to calculate the average amplitude spectrum of the data before and after deconvolution, as shown in figure 9. Figure 9 confirms that the average amplitude spectrum of the seismic section after being processed by the streaming PEF deconvolution is broader than that of the traditional deconvolution result and slightly narrower than that of the iterative deconvolution result in the effective frequency range. However, according to the computation time of the different deconvolution methods, the computational efficiency of the proposed method is significantly improved compared with the iterative method. It further verifies the effectiveness and high efficiency of the streaming PEF deconvolution method in processing nonstationary seismic data.

CONCLUSION

We have improved the theory of streaming PEF with temporal and spatial constraints and proposed a multichannel adaptive deconvolution based on streaming PEF in the time-space domain. Our approach uses a time-varying prediction step to guarantees the reasonable amplitude relationship of deconvolution results. The proposed method updates the filter coefficients simultaneously when each new data point arrives, which effectively represents the nonstationary characteristics of the seismic data. The efficient computational feature of streaming computation is useful for efficient adaptive deconvolution in high-dimensional data processing. Synthetic examples and field data test confirm that the proposed deconvolution method is successful in enhancing the temporal resolution of seismic data while preserving the relative amplitude relationship and structural continuity.

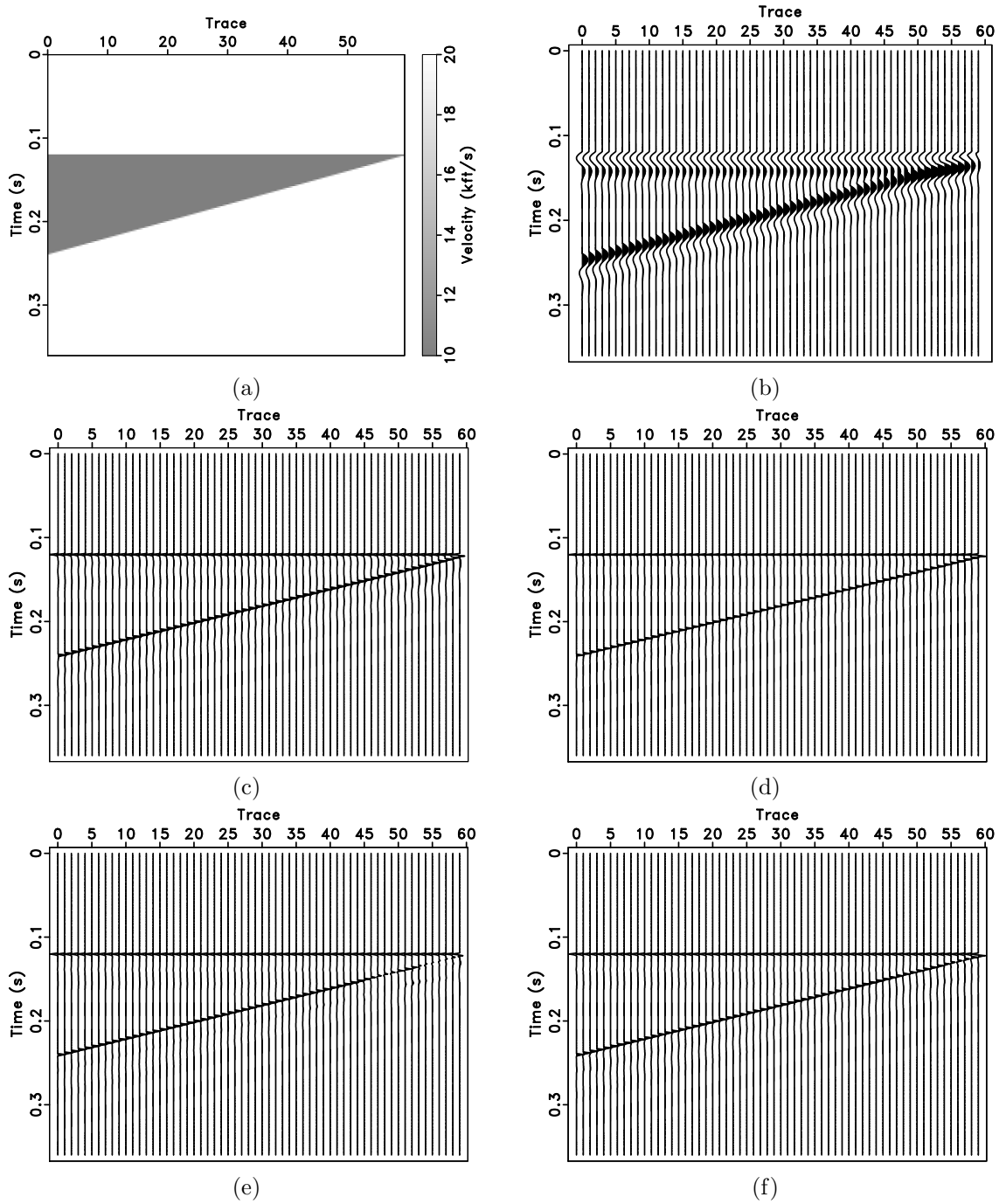


Figure 7: Wedge model. Wedge velocity model (a), synthetic data (b), the result of traditional predictive deconvolution (c), the result of iterative deconvolution (d), the result of adaptive single-channel deconvolution without spatial constraint (e), the result of adaptive multichannel deconvolution with spatial constraint (f).

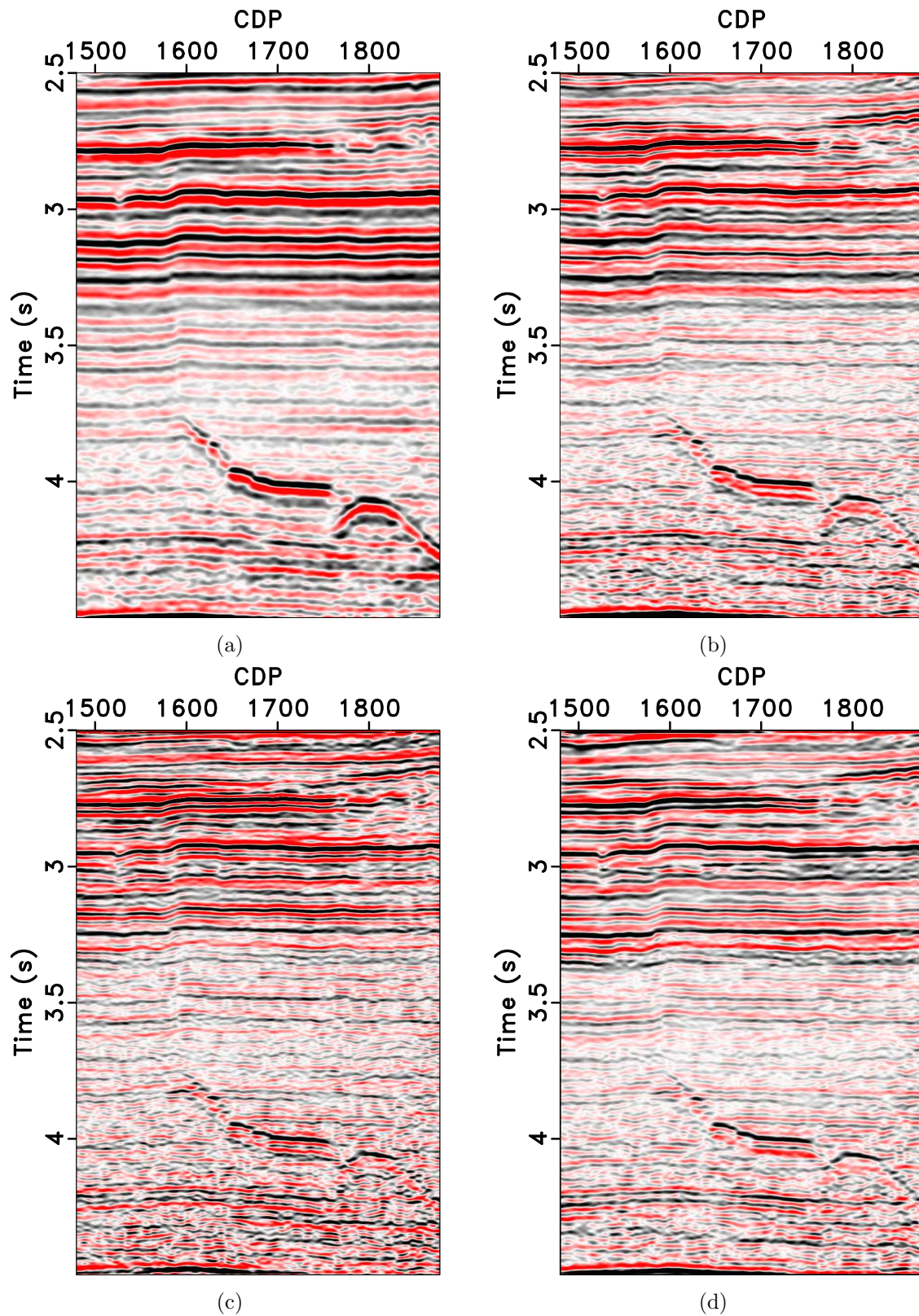


Figure 8: Deconvolution results by using different methods. Poststack field data (a), traditional predictive deconvolution (b), iterative deconvolution (c), streaming PEF deconvolution (d).

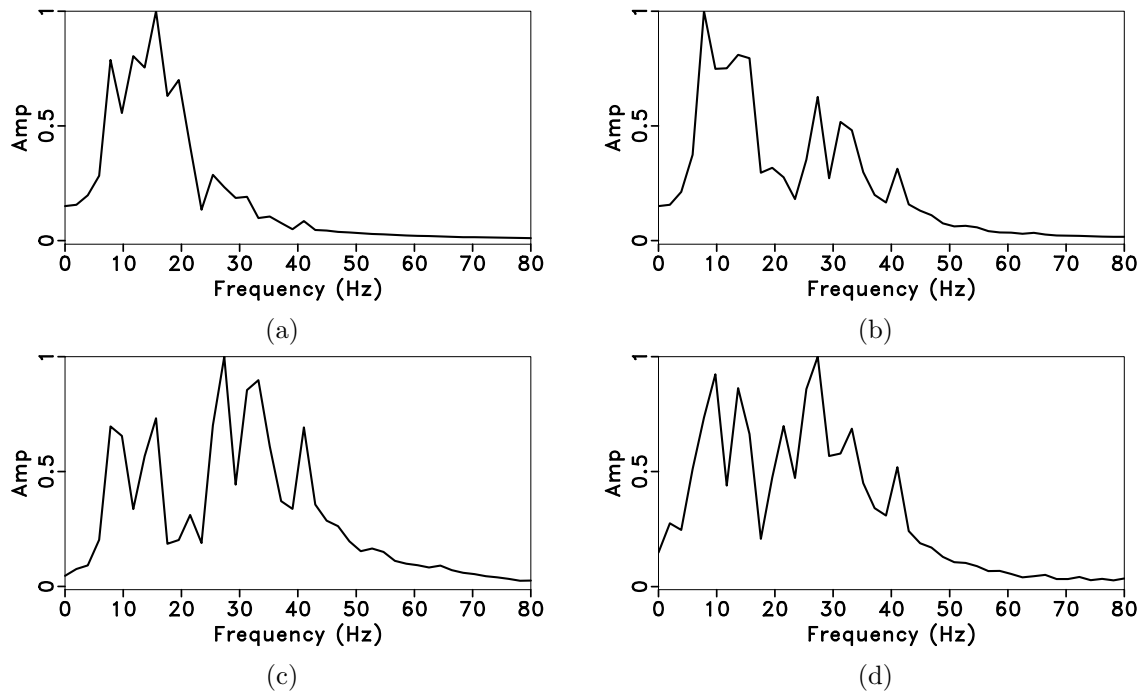


Figure 9: Comparison of the average amplitude spectrum of the deconvolution results and original field data. Original field data (a), traditional predictive deconvolution (b), iterative deconvolution (c), streaming PEF deconvolution (d).

ACKNOWLEDGMENTS

This work is supported by Nation Natural Science Foundation of China (grant nos. 41974134 and 41774127).

REFERENCES

- Claerbout, J. F., 1992, Fundamentals of geophysical data processing with application to petroleum prospecting: McGraw-Hill Inc.
- Clark, G. K. C., 1968, Time-varying deconvolution filters: *Geophysics*, **33**, 936–944.
- Fomel, S., 2007a, Local seismic attributes: *Geophysics*.
- , 2007b, Shaping regularization in geophysical-estimation problems: *Geophysics*.
- Fomel, S., and J. Claerbout, 2016, Streaming prediction-error filters: 86th Annual International Meeting, SEG, Expanded Abstracts, 4787–4791.
- Griffiths, L. J., F. R. Smolka, and L. D. Trembly, 1977, Adaptive deconvolution: A new technique for processing time-varying seismic data: *Geophysics*, **42**, 742–759.
- Hager, W. W., 1989, Updating the inverse of a matrix: *SIAM Review*, **31**, 221–239.
- Koehler, F., and M. T. Taner, 1985, The use of the conjugate-gradient algorithm in the computation of predictive deconvolution operators: *Geophysics*, **50**, 683–695.
- Li, F., S. D. Wang, X. H. Chen, G. C. Liu, and Q. Zheng, 2013, Prestack nonstationary

- deconvolution based on variable-step sampling in the radial trace domain: *Applied Geophysics*, **10**, 423–432.
- Li, Z. X., Z. C. Li, and W. K. Lu, 2016, Multichannel predictive deconvolution based on the fast iterative shrinkage-thresholding algorithm: *Geophysics*, **81**, V17–V30.
- Liu, Y., and S. Fomel, 2011, Seismic data interpolation beyond aliasing using regularized nonstationary autoregression: *Geophysics*, **76**, V69–V77.
- Liu, Y., and B. X. Li, 2018, Streaming orthogonal prediction filter in the t-x domain for random noise attenuation: *Geophysics*, **83**, F41–F48.
- Margrave, G. F., M. P. Lamoureux, and D. C. Henley, 2011, Gabor deconvolution: Estimating reflectivity by nonstationary deconvolution of seismic data: *Geophysics*, **76**, W15–W30.
- Peacock, K. L., and S. Treitel, 1969, Predictive deconvolution: theory and practice: *Geophysics*, **34**, 155–169.
- Porsani, M. J., and B. Ursin, 2007, Direct multichannel predictive deconvolution: *Geophysics*, **72**, H11–H27.
- Prasad, S., and A. K. Mahalanabis, 1980, Adaptive filter structures for deconvolution of seismic signals: *IEEE Transactions on Geoscience and Remote Sensing*, 267–273.
- Ristow, D., and D. Jurczyk, 1975, Vibroseis deconvolution: *Geophysical Prospecting*, **23**, 363–379.
- Robinson, E. A., 1957, Predictive decomposition of seismic traces: *Geophysics*, **22**, 767–778.
- , 1967, Predictive decomposition of time series with application to seismic exploration: *Geophysics*, **32**, 418–484.
- ver der Baan, M., 2008, Time-varying wavelet estimation and deconvolution by kurtosis maximization: *Geophysics*, **73**, V11–V18.
- , 2012, Bandwidth enhancement: Inverse Q filtering or time-varying wiener deconvolution: *Geophysics*, **77**, V133–V142.
- Wang, R. J., 1969, The determination of optimum gate length for time-varying wiener filtering: *Geophysics*, **34**, 683–695.
- Wang, Y. H., 2002, A stable and efficient approach to inverse Q filtering: *Geophysics*, **67**, 657–663.
- , 2006, Inverse Q-filter for seismic resolution enhancement: *Geophysics*, **71**, V51–V60.
- , 2008, *Seismic inverse Q filtering*: Blackwell, Oxford.
- Wang, Y. H., and J. Guo, 2004, Modified kolsky model for seismic attenuation and dispersion: *Journal of Geophysics and Engineering*, **1**, 187–196.